IEEE Access
Multidisciplinary ⋮ Rapid Review ⋮ Open Access Journal

Received 23 February 2023, accepted 13 March 2023, date of publication 16 March 2023, date of current version 14 November 2023.

Digital Object Identifier 10.1109/ACCESS.2023.3257996

RESEARCH ARTICLE

Evaluation and Test of Impact-Resistant Overload Capability of Companion-Type Direct Cooling Motor

QIANG HOU[1], YUEJUN AN[1], MING LI[1,2], HUI AN[1], NING SUN[1], CHANGLIN LIU[1], AND YANJUN LU[3]

[1]School of Electrical Engineering, Shenyang University of Technology, Shenyang 110000, China
[2]School of Engineering, Bohai University, Jinzhou 121000, China
[3]Shenyang Kingsem Company Ltd., Shenyang 110000, China

Corresponding author: Yuejun An (anyj_dq@sut.edu.cn)

This work was supported by the Science and Technology Major Projects in Liaoning Province of China under Grant 2022JH1/10400038.

ABSTRACT In the actual working process of the motor, there will be short-term overload conditions, which puts forward higher requirements for maintaining the overload capacity of the motor. Due to the limitation of the thermal limit on the overload capacity of the motor, taking a 250kW permanent magnet synchronous motor (PMSM) as an example, this paper proposes a thermal management scheme of companion-type direct cooling, and establishes a three-dimensional thermal network model considering the secondary circulation factor. At the same time, in order to explore the influence of the thermal management scheme on the overload capacity of the motor when there is an impact load, on the premise that there is a safety margin for the hottest spot temperature of the winding under the rated state of the motor, the impact load is simulated by setting the overload torque, the thermal network model is used to compare and analyze the temperature field of the motor based on the companion-type direct cooling and the indirect casing cooling, and combining with the insulation limit to quantitatively compare the overload capacity of the motor after impact load. Through the simulation test, it is verified that the motor based on the companion-type direct cooling has efficient heat dissipation and stronger impact-resistance overload capability. The proposal of the companion-type direct cooling scheme has important practical significance for excavating the load potential of the motor under actual operating conditions.

INDEX TERMS Companion-type direct cooling, secondary circulation, high-precision three-dimensional thermal network, impact load, evaluation of overload capacity, simulation test.

I. INTRODUCTION

With the promotion of international requirements for energy saving and environmental protection, the energy consumption standards formulated by China have been continuously improved, and higher requirements have been put forward for motor performance indicators such as efficiency, power density, impact-resistance overload capability and reliability [1]. During the actual operation of the motor, there will be intermittent sudden changes in the load. At this time, the motor needs to have a high torque overload capacity under the condition of constant speed [2]. However, the increase of the electromagnetic torque requires the drive motor to increase the electrical load. The increase of the electrical load will lead to an increase in the Joule loss, which further increases the heat generation of the motor. At the same time, when the output torque of the motor increases to a certain level, due to the limited size of the motor, the heat is difficult to dissipate, resulting in serious heat generation of the motor [3].

If the temperature of the motor is too high, the insulation in the slot may be aged, and the windings may be short-circuited between turns or phases, which will affect the service life

The associate editor coordinating the review of this manuscript and approving it for publication was Zhuang Xu.

and reliability of the motor. At the same time, the magnetism of the permanent magnet will gradually decrease with the increase of temperature. When the temperature rises to the Curie temperature, the magnetization will disappear, resulting in irreversible demagnetization of the permanent magnet, which will seriously affect the performance of the motor or even fail to operate. It can be seen that the problem of heat dissipation in the effective space has become a bottleneck for the further improvement of the motor's impact-resistance overload capability [4], so efficient thermal management is required to prevent the motor from exceeding the insulation thermal level. For a given insulation limit in the stator slot, in the face of short-term overload conditions of the motor, efficient thermal management will allow higher current density, thereby increasing the motor output torque in an effective space volume.

The traditional forced air cooling system uses fans to cool down the motor, but for a high-torque motor with a large current density, the low heat dissipation efficiency limits the output torque capability of the motor [5]. Therefore, using high thermal conductivity fluid and optimizing the design of the thermal conduction path is an effective thermal management method to solve the temperature rise of the motor. A common thermal management method is to integrate a cooling tube inside the casing or the yoke of the stator core, which has better heat dissipation and less impact on electromagnetic performance [6], [7], [8], [9]. However, the water pipes are usually arranged far away from the windings and permanent magnets, which are the main heat sources, increasing the thermal resistance of the heat dissipation path. At the same time, the end winding cannot transfer heat through the stator core in a heat conduction way, resulting in the hottest point of the motor at the end of the winding. In order to reduce thermal resistance, motor designers even use oil-cooled heat dissipation in which the coolant is in direct contact with the heat source, which greatly reduces the thermal resistance of the high-heating parts of the motor, and also solves the problem of difficult heat dissipation at the end. However, the viscosity of the oil is large, which increases the energy loss when the rotor rotates. At the same time, the oil medium needs to be strictly filtered, so as to avoid the damage to the insulation layer of the motor caused by impurities in the oil, and the sealing requirements of the motor are also high, which increases the cooling system design cost [10], [11], [12], [13]. Motor designers have even placed cooling pipes in the unused space in the stator slots to directly cool the winding heat source, which is closer to the windings and permanent magnets than the water jacket cooling method, showing excellent cooling performance [4]. In addition to the above thermal management solutions, the motor designers proposed the solution of multi-turn winding twisted in cooling tube, which further reduced the temperature rise of the windings evenly and greatly improved the heat dissipation efficiency of the motor. However, due to the bending of the cooling steel pipe, it brings certain challenges to the winding of the outer layer of the pipe, and the maximization of the efficiency of the cooling system and the manufacturing feasibility are not considered [14], [15].

The existing reports have done a lot of research on various thermal management schemes and evaluation methods of heat dissipation capacity, but there are still the following problems to be solved:

1) There are insulating materials such as insulating paint, insulating paper and epoxy resin in the stator slot of the motor, which increases the thermal resistance between the winding heat source and the external environment. There are few reasonable solutions to this problem in the existing thermal management reports of the motor.

2) In the cooling performance evaluation method of thermal management scheme, the finite element method is used to analyze the thermal performance of motor in references [6], [7], and [11]. The calculation accuracy is high, but it affects the engineering application because it takes up a lot of calculation resources. In references [16] and [17], the two-dimensional thermal network model is used to predict the temperature of each part of the motor, which has the advantage of short calculation period, but in the practical engineering application, there is a big gap between the cooling performance of each part and the actual. Although the existing commercial software Motor-cad can use three-dimensional thermal network model to accurately predict the motor temperature, it can not be calculated and analyzed effectively for the new thermal management scheme. In references [18], [19], and [20], the three-dimensional thermal network model is used to evaluate the thermal performance of the motor, and the anisotropy of different materials is considered. Compared with the two-dimensional thermal network model, the evaluation accuracy is improved in advance with a short calculation cycle. However, for the thermal management scheme of spiral channel, the existing three-dimensional thermal network model does not take into account the influence of secondary circulation on the mainstream boundary layer. There is a certain gap between the temperature of each part of the motor and that of the actual running state.

3) The load sudden change will occur in the actual operation of the motor, so it is very important to make full and rational use of the continuous load energy of the motor under the impact load. In references [21], [22], and [23], the short-term thermal transient of motor under overload condition is predicted by thermal model, and the impact-resistance overload capability of motor is evaluated effectively. However, the direct relationship between thermal resistance of different thermal management schemes and motor torque output capacity has not been theoretically studied, and the selection of motor thermal management scheme under different load sudden change conditions can not be reasonably evaluated.

In order to improve the cooling performance and torque output ability of the motor to a greater extent, from the perspective of reducing the thermal resistance between the cooling medium and the heat source, excellent thermal

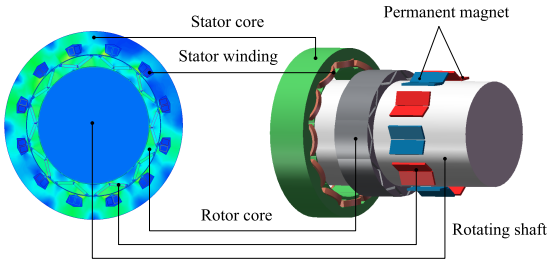

FIGURE 1. Topology of the proof-of-concept PMSM motor.

management scheme and evaluation method of cooling performance are proposed. The main contributions are three-fold:

1) The thermal management scheme of the companion-type direct cooling is proposed. The cooling pipe is twined in the stator slot with the each turn winding, and the multiple outer surfaces of each stator winding are directly and seamlessly contacted with the cooling pipe wall. The heat generated by the loss of the winding does not need to pass through the insulation material in the stator slot.

2) Since the circumferential heat transfer has a great influence on the heat dissipation of the motor, and because of the particularity of the structure of the companion-type direct cooling scheme, a three-dimensional thermal network model of omnidirectional heat transfer is established based on the traditional two-dimensional thermal network model of radial-axial heat transfer, and the influence of secondary circulation on the mainstream of cooling medium is considered. At the same time, the finite element method is used to verify the effectiveness and accuracy of the three-dimensional thermal network model considering secondary circulation.

3) The direct influence of thermal resistance on the torque output capability of the motor under the winding limit temperature constraint is theoretically deduced and analyzed, and the impact-resistance overload capability of the motor under the companion-type direct cooling scheme and indirect casing cooling scheme is quantitatively studied and compared. At the same time, a simulation prototype is designed to verify the cooling performance and load potential of the two thermal management schemes.

II. PROPOSAL OF COMPANION-TYPE DIRECT COOLING SCHEME

A. DESIGN OF PROOF-OF-CONCEPT MOTOR

This paper takes a 250kW permanent magnet synchronous motor (PMSM) motor as the research object. The motor adopts a rotor structure with built-in permanent magnets, and a concentrated flat wire winding is wound in the stator slot. The windings are arranged in the slot compactly and Neat, reducing the gap between the windings in the same stator slot, and reducing the heat transfer resistance between the windings, so that the heat generated by the winding loss is relatively easy to transfer to the casing. The topology of the designed proof-of-concept PMSM motor is shown in Fig.1.

TABLE 1. Key electrical and dimensional parameters of the proof-of-concept PMSM motor.

Specifications	Values
Rated power P_N (kW)	250
Based speed n_N (r/min)	600
Rated voltage U_N (V)	542
Maximum torque T_{max} (N·m)	6000
Rated power factor cosφ	0.92
Rated efficiency η (%)	98
Based frequency f (Hz)	50
Stator slots/PM pole-pair Z/P	10/6
Outer diameter of outer stator D_{so} (mm)	1060
Inner diameter of outer stator D_{si} (mm)	800
Length of core L_a (mm)	250
Maximum operating temperature of insulation T (°C)	130
Copper Loss P_{cu} (W)	2314
Iron loss P_{Fe} (W)	1217
Permanent Magnet Eddy Current Loss P_w (W)	186

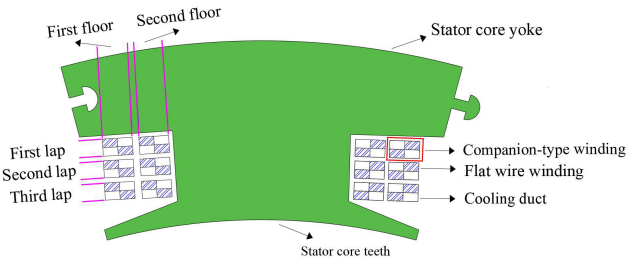

FIGURE 2. Schematic diagram of the companion-type direct cooling scheme.

The stator core in the proof-of-concept PMSM motor adopts single-tooth splicing, which is beneficial to the realization and manufacture of the companion-type direct cooling thermal management solution, as well as the improvement of material utilization and cost reduction. The main electrical properties and dimensional parameters of the proof-of-concept PMSM motor are listed in Table 1.

B. DESIGN OF THERMAL MANAGEMENT SOLUTIONS

Based on the design of the proof-of-concept PMSM motor, when the motor is overloaded for a short time, in order to improve the limitation of the thermal limit on the overload capacity of the motor, this paper proposes a thermal management scheme of companion-type direct cooling. Companion-type hybrid windings are arranged in the stator slots, two cooling tubes and two copper conductors are distributed diagonally, and four hybrid-type windings are wound on the stator teeth in parallel. In order to increase the heat exchange area between the cooling pipe and the copper conductor, and make the winding of the four flat bodies more convenient in the process, the cooling pipe and the copper conductor are designed to be the same size. The schematic diagram of the companion-type direct cooling scheme in Fig.2.

The parallel winding process for companion-type windings in Fig.3. The cooling tube and the copper conductor are wound in parallel from the bottom slot on the right side of the stator teeth to the slot on the left side. After a lap

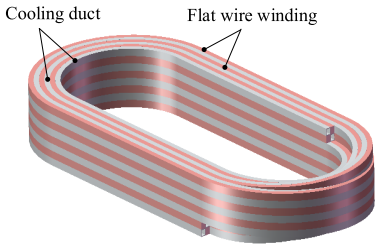

FIGURE 3. Schematic diagram of parallel winding of companion-type windings.

is completed, companion-type windings are staggered at a certain height at the end of the stator and wound down from the first lap to the second lap. After the winding of the first floor is completed, the first lap of the second floor is wound in parallel at the inclined shoulder of the stator slot. After the first lap of the second layer is finished, the second lap is still twisted upward at a certain height at the end of the stator until the winding of the four companion-type windings of the second layer is finished. Due to the limitation of the size of the companion-type winding and the stator slot, the companion-type winding proposed in this paper adopts a three-floor four-lap system in practical application. As can be seen from Fig.3, whether it is a companion-type winding in the stator slot or at the stator end, the tubes between floors and between laps are in contact with each other. At the same time, multiple surfaces of the copper conductor are contacted with the cooling tube, and the winding is as if immersed in the coolant.

The eddy current loss on the surface of the cooling tube only accounts for 0.02% of the output power of the proof-of-concept PMSM motor due to the mutual suppression and cancellation of the induced potential formed by the copper conductor around the cooling tube on its surface. The eddy current loss has little effect on the loss of the motor under normal operation. In order to reduce the complexity of the three-dimensional thermal network model proposed in this paper, the eddy current loss of the cooling tube is ignored in the subsequent research.

Since the alternating current frequency of proof-of-concept PMSM motor is 50 Hz, and the stator slot winding adopts the method of multiple strands of fine wire winding, the skin effect has little effect on the stator winding resistance value, which can be ignored in the subsequent research and calculation.

III. ESTABLISHMENT OF THREE-DIMENSIONAL THERMAL NETWORK MODEL

In order to demonstrate the feasibility of the proposed thermal management scheme, and to facilitate the subsequent optimization and quantitative analysis of the thermal management scheme, a three-dimensional thermal network analysis model considering secondary circulation is proposed in this section, which can quickly and accurately predict the temperature distribution of various components of the motor.

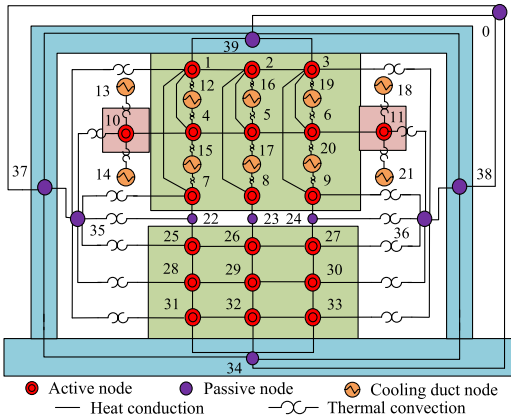

FIGURE 4. Axial-radial thermal network model diagram for companion-type direct cooling scheme.

At the same time, in order to compare the efficient cooling performance of the companion-type direct cooling scheme, a three-dimensional thermal network model considering secondary circulation is established for the indirect casing cooling.

A. ESTABLISHMENT OF THREE-DIMENSIONAL THERMAL NETWORK MODEL

In order to simplify the solution process, based on the principles of heat mass transfer and the characteristics of the thermal network, the following basic assumptions are made in the modeling and solution process [24], [25]:

1) The surface heat dissipation coefficient of each component of the motor is constant, ignoring the change of thermal conductivity and heat dissipation coefficient with temperature;

2) The copper loss caused by the skin effect and the proximity effect of the winding is ignored, and the eddy current loss caused by the metal cooling pipe is ignored;

3) The stator and rotor iron losses and permanent magnet eddy current losses of the motor do not change with temperature.

A discrete axial-radial thermal network model is established for the thermal management scheme of companion-type direct cooling and indirect casing cooling, as shown in Fig.4 and Fig.5 respectively. The node 0 in the figure represents the ambient temperature, and the active nodes are: 1-3 are the nodes of the yoke of the stator core, 4-6 are the winding nodes in the stator slot, 7-9 are the nodes of the teeth of the stator core, and 10-11 are the end winding nodes of the stator, 25-27 are the upper nodes of the rotor core, 28-30 are the permanent magnet nodes, and 21-33 are the lower nodes of the rotor core. Passive nodes include: 12-21 are cooling conduit nodes, 22-24 are air gap nodes, 34 are shaft nodes, 35-36 are end air cavity nodes, 37-38 are end cap nodes, and 39 is a casing node.

The thermal network in Fig.4 only considers the radial-axial heat transfer, but the companion-type direct

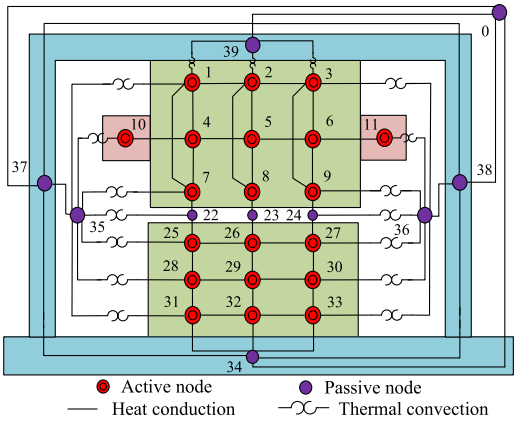

FIGURE 5. Axial-radial thermal network model diagram for indirect casing cooling scheme.

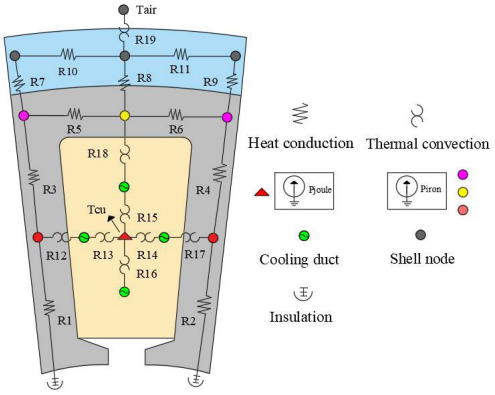

FIGURE 6. Radial-circumferential thermal network model diagram of companion-type direct cooling motor.

cooling scheme established in this paper has a great influence on the circumferential heat transfer of the winding and stator core. At the same time, the materials of different parts of the motor have heat transfer anisotropy, which also has a great influence on the circumferential heat transfer. Therefore, in order to more accurately predict the temperature rise of each component based on the companion-type direct cooling motor, based on the axial-radial thermal network, a thermal network model considering circumferential heat transfer is established in this paper, as shown in Fig.6. For clarity, only a radial-circumferential thermal network model of the stator slots and windings in the slots is shown [26], [27]. In this paper, an axial-radial thermal network model based on the indirect casing cooling scheme is also established, which is no longer shown here.

B. CALCULATION OF THERMAL RESISTANCE

Based on the proposed thermal management scheme, in order to obtain simple but physically meaningful results, the stator teeth and stator windings are treated as flat conductors, and the casing and stator yoke are treated as cylindrical conductors.In this section, the thermal resistance of the

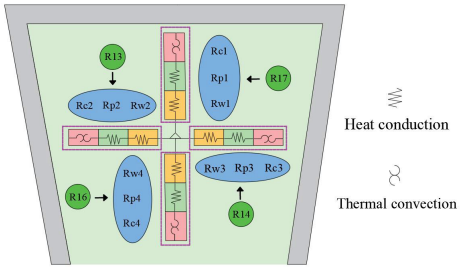

FIGURE 7. Single thermal network of stator windings and cooling tubes.

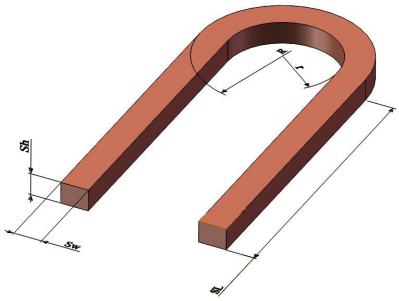

FIGURE 8. The size of the stator winding after equivalent to a single thermal network.

companion-type direct cooling is analyzed and calculated in detail, and the thermal resistance calculation based on the indirect casing cooling is calculated according to the formula of this section.

The companion-type winding has multiple turns in a single stator slot, but due to its unique winding method, all stator windings and cooling tubes in each slot are equivalent to a single thermal network, as shown in Fig.7. The radial-circumferential thermal resistance (R13-R16 in Fig.6) between the stator winding node and the cooling tube node is classified and solved: 1) The internal heat transfer resistance Rw of the stator winding; 2) The heat transfer thermal resistance Rp between the cooling tube wall and the stator winding; 3) The heat transfer thermal resistance Rc between the cooling tube wall and the cooling medium, so as to obtain the precise thermal resistance parameters.

The size of stator winding equivalent to a single thermal network is shown in Fig 8, where Sh is the height of the stator winding, Sw is the width of the stator winding, SL is the length of the half-turn stator winding, and r and R are the inner radius and outer radius of the stator end winding respectively. The thermal resistance Rw1-Rw4 is calculated by Eq. (1), and kw is the equivalent thermal conductivity of the stator winding [26].

$$R_{w1} = R_{w4} = \frac{S_h}{2S_w(S_L + \pi R_e)k_w}$$
$$R_{w2} = R_{w3} = \frac{S_w}{2S_h(S_L + \pi R_e)k_w} \quad (1)$$

Since there are insulating materials such as insulating paint and epoxy resin in the stator slots, in order to

simplify the calculation model, the stator winding is modeled as a composite material composed of insulators and copper conductors. Therefore, the stator winding homogenization method of Hashin and Shtrickman is used, and the equivalent thermal conductivity is calculated by Eq. (2) [28].

$$k_w = k_{re}\frac{(1+k_{cu})k_{cu}+(1-k_{cu})k_{re}}{(1-k_{cu})k_{cu}+(1+k_{cu})k_{re}} \tag{2}$$

where k_re and k_{cu} are the thermal conductivity of the insulator and copper conductor respectively.

The contact thermal resistance R_{p1}-R_{p4} between the cooling tube wall and the stator winding is calculated by Eq. (3), and the contact area between the two is determined by the contact factor cf between the cooling tube and the winding [26].

$$\begin{aligned} R_{p1} = R_{p4} &= \frac{h_{air}}{S_w(S_L+\pi R)k_{air}c_f} \\ R_{p2} = R_{p3} &= \frac{h_{air}}{S_h\cdot(S_L+\pi R)\cdot k_{air}\cdot c_f} \end{aligned} \tag{3}$$

where h_{air} is the air thickness between the cooling tube and the stator winding, and k_{air} is the thermal conductivity of the air.

Since the cooling pipe in the companion-type direct cooling scheme is spiral, the centrifugal force generated by the cooling medium flowing in the pipe will form a secondary circulation in the flow field, which is perpendicular to the main flow, which increases the disturbance to the boundary layer and is conducive to heat dissipation. In order to more accurately analyze the convective heat transfer state between the cooling medium and the inner wall of the pipe, this paper considers the influence of the secondary circulation on the main flow on the basis of the traditional calculation of the convective heat transfer coefficient, and the convective heat transfer coefficient of the inner surface of the cooling pipe is calculated by Eq. (4) [29].

$$k_w = \frac{N_u\lambda}{d_{wet}}\varepsilon_R \tag{4}$$

where N_u is the Nusselt number, λ is the thermal conductivity of water, and d_{wet} is the equivalent diameter of the cooling pipe. ε_R is the secondary circulation influence factor, which is calculated by Eq. (5) [29].

$$\varepsilon_R = 1+10.3(\frac{d}{R})^3 \tag{5}$$

where R is the average radius of curvature of the cooling pipe, and d is the diameter of the cooling pipe.

After obtaining the precise convective heat transfer coefficient, the thermal resistance between the cooling tube wall and the cooling medium can be obtained from Eq. (6) [29].

$$\begin{aligned} R_{c1} = R_{c4} &= \frac{1}{S_w(S_L+\pi R)k_w} \\ R_{c2} = R_{c3} &= \frac{1}{S_h(S_L+\pi R)k_w} \end{aligned} \tag{6}$$

Therefore, the radial-circumferential thermal resistances between the stator winding node and the cooling tube node can be calculated by Eq. (7) respectively.

$$\begin{aligned} R_{15} = R_{16} &= R_{w1}+R_{p1}+R_{c1} \\ R_{13} = R_{14} &= R_{w2}+R_{p2}+R_{c2} \end{aligned} \tag{7}$$

According to the calculation formula of the thermal resistance of the plate conductor and the cylindrical conductor in the thermal resistance network, the other thermal resistances in Fig. 6 are calculated according to the Eq. (8) - Eq. (11) [24].

$$\begin{aligned} R_{12} = &\frac{ZS_w}{2k_w(D_{so}-D_{si})/2-d_y)L_a} \\ &+\frac{Zb_t}{2k_{core}(D_{so}-D_{si})/2-d_y)L_a} \end{aligned} \tag{8}$$

$$\begin{aligned} R_{18} = &\frac{Z}{2\pi k_{core}L_a\ln\left[(D_{so}-d_y)/(D_{so}-2d_y)\right]} \\ &+\frac{Z}{2\pi k_wL_a\ln\left[(D_{so}-2d_y)/D_{si}\right]} \end{aligned} \tag{9}$$

$$\begin{aligned} R_3 = &\frac{Z}{2\pi k_{core}L_a\ln\left[(D_{so}-d_y)/(D_{so}-2d_y)\right]} \\ &+\frac{Z(D_{so}-d_y-D_{si})}{2k_{core}t_wL_a} \end{aligned} \tag{10}$$

$$\begin{aligned} R_8 = &\frac{1}{2\pi k_jL_a\ln\left[D_{so}/(D_{so}+h_j/2)\right]} \\ &+\frac{1}{2\pi k_{core}L_a\ln\left[(D_{so}-d_y)/(D_{so})\right]} \end{aligned} \tag{11}$$

where k_{core} is the thermal conductivity of the stator core, k_j is the thermal conductivity of the casing, and h_j is the thickness of the casing.

For the stator and rotor silicon steel laminations, the thermal conductivity of the insulating layer between the sheets in the axial direction is much lower than that of the silicon steel sheet itself, and the thickness difference is also very large, so the equivalent model is used for the stator and rotor cores. In order to simplify the calculation model and improve the calculation accuracy, this paper refers to the idea of [26] and the stator and rotor silicon steel sheets are axially layered and equivalently calculated. The equivalent model is a heat transfer body in which silicon steel sheets and insulating layers between sheets are alternately arranged. According to the principle of equal heat generation and constant heat dissipation, the thermal conductivity of the equivalent thermal conductor can be calculated according to Eq. (12). Considering that the lamination coefficient of the stator lamination is 96%, the ratio of the thickness of the insulating layer to the thickness of the silicon steel sheet is 1:24.

$$k_e = \frac{d_s+d_n+\cdots+d_s+d_n}{\frac{d_s}{k_s}+\frac{d_n}{k_n}+\cdots+\frac{d_s}{k_s}+\frac{d_n}{k_n}} \tag{12}$$

where k_s and d_s are the thermal conductivity and thickness of the silicon steel sheet respectively, k_n and d_n are the thermal conductivity and thickness of the insulating layer between the sheets respectively.

The stator core is equivalently divided into three sections in the axial direction, then the axial thermal resistance of the stator core is calculated according to Eq. (13) [26].

$$R_z = \frac{4}{3\pi k_e \left[D_{so}^2 - \left(D_{so} - 2d_y\right)^2\right]} + \frac{2}{3k_e b_t Z \left(D_{so} - D_{si} - 2d_y\right)} \tag{13}$$

IV. EFFECT OF THERMAL RESISTANCE ON TORQUE OUTPUT CAPACITY

A. DETERMINATION OF LOSS

Since the temperature point of most concern in this paper is on the stator winding, which is surrounded by the stator yoke and stator teeth, the stator core loss will cause the winding temperature to rise. In order to consider the influence of different loss positions, the core loss is divided into two parts: the stator yoke loss P_{sy} and the stator tooth loss P_{st}. In addition, considering the effect of rotor losses on the temperature rise of the stator windings, the permanent magnet eddy current losses are also taken into account.

1) Copper loss of stator winding

Since the winding temperature is considered as the optimal thermal boundary condition, the resistance value should naturally take into account the effect of temperature. After the cross-sectional area and length are known, the winding loss is calculated by Eq. (14) [28], [30].

$$P_{cu} = 3{I_a}^2 \rho_0 (1 + \alpha_{cu} T_{cu}) \frac{2N_w(L_a + L_e)}{aA_s} \tag{14}$$

where I_a is the winding phase current, ρ_0 is the copper resistivity at 0°C, α_{cu} is the temperature coefficient, T_{cu} is the estimated winding temperature, $A_s$is the winding cross-sectional area, a is the number of parallel branches, N_w is the number of turns in series per phase and $L_e$is the winding end length, $L_e = (R + r)/2$.

2) Loss of stator core

The stator core losses include hysteresis losses, eddy current losses and additional losses. Assuming that the magnetic flux density waveform is sinusoidal and ignores the influence of the armature reaction, the stator core loss can be calculated by the Bertotti model by Eq. (15) [28].

$$p_{Fe} = k_h f B_m^2 + k_e {f^2} B_m^2 + k_{exc} {f^{1.5}} B_m^{1.5} \tag{15}$$

where k_h, k_e and k_{exc} are the corresponding coefficients obtained by fitting the loss curve given by the manufacturer. Through the method of numerical analysis, calculate the magnetic density value B_m in any finite area in the core, and substitute it into the Eq. (15) to calculate the core loss density p_{Fe}.

Simplifying the shape of the stator teeth and ignoring the loss of the stator tooth tip, the loss of the stator teeth and yoke can be calculated by Eq. (16) [28].

$$\begin{aligned} P_{st} &= p_{Fe} L_a N_s b_t \left(\frac{D_{so} - D_{si}}{2} - b_y\right) \\ P_{sy} &= \frac{\pi}{4} p_{Fe} L_a \left[D_{so}^2 - (D_{so} - 2b_y)^2\right] \end{aligned} \tag{16}$$

where b_t is the width of the stator top, and b_y is the thickness of the stator yoke.

3) Eddy current loss of magnet

The eddy current loss in the magnet under load is mainly generated by the higher harmonic cutting in the armature magnetomotive force, which can be calculated according to the classical eddy current loss Eq. (17) [28].

$$P_w = \frac{1}{24} \sigma \omega^2 d^2 B_{av}^2 F \left(\frac{d}{\Delta}\right)] \tag{17}$$

where σ is the conductivity of the magnetic steel, and ω is the frequency of the magnetic field, and d is the thickness of the magnetic steel, and B_{av} is the average magnetic density, and Δ is the penetration depth,$\Delta = \sqrt{2/(\omega\mu\sigma)}$.

B. INFLUENCE OF THERMAL RESISTANCE ON OUTPUT TORQUE

The heat balance equation of the three-dimensional thermal network model can be easily established according to the Kirchhoff law. To determine the temperature at each node, Eq. (18) can be solved [28], [31].

$$AX = B \tag{18}$$

where A is the heat conduction matrix, X is the temperature matrix containing the temperature at each node, and B is the loss matrix containing the losses at each node.

$$\Delta\theta_m = \sum_{n=1}^{k} \left[A^+(m, n) - A^+(1, n)\right] B(n, 1) \tag{19}$$

The temperature rise of any node m relative to the environment can be obtained by Eq. (19) [28], where A + is the Moore-Penrose generalized inverse of A. By calculating Eq. (18) and Eq. (19), the temperature rise result of the stator winding can be obtained from Eq. (20) [24].

$$\Delta\theta_{cu} = k_1 P_{cu} + k_2 (P_{st} + P_w) + k_3 P_{sy} \tag{20}$$

where k_1, k_2 and k_3 are the relational expressions composed of thermal resistance between different nodes.

It can be seen from Eq. (20) that not only the copper loss, but also the stator core loss and the permanent magnet eddy current loss also lead to the increase of the winding temperature. The contribution to the temperature rise of the windings depends on the different loss values and the thermal resistance between the nodes of the different motor components. In addition, Eq. (20) also provides an understanding of the mathematical relationship between losses and thermal resistance and the temperature rise of the stator windings. Therefore, the maximum allowable copper loss under the

limit of the temperature rise of the stator winding can be calculated by Eq. (21) [24].

$$P_{cu} = \frac{\Delta\theta_{cu}}{k_1} - \frac{k_2}{k_1}(P_{st} + P_w) - \frac{k_3}{k_1}P_{sy} \tag{21}$$

Since the reluctance torque of PMSM motors with concentrated windings is usually negligible [32], when the air-gap flux density distribution is uniform and the influence of armature reaction is ignored, its electromagnetic torque can be calculated by Eq. (22) [24].

$$T = 2D_{so}L_aN_wI_aB_g \tag{22}$$

where B_g is the air gap magnetic flux density.

It is assumed that the stator iron loss and permanent magnet eddy current loss do not change with temperature, and the electromagnetic load and the size of each component under different cooling methods remain unchanged, that is, P_{st},P_{sy} and P_w are constants.

Therefore, when the external dimensions of the prototype remain unchanged, Eq. (14) and Eq. (21) are substituted into Eq. (22), and then the electromagnetic torque can be conveniently expressed as a function of the loss and thermal resistance based on the winding temperature constraint, such as Eq. (23) is shown.

$$T = 2D_{so}L_aN_wB_g\sqrt{\frac{\left[\Delta\theta_{cu} - k_2\left(P_{st} + P_w\right) + k_3P_{sy}\right]A_s}{6N_w^2\rho_0\left(1 + \alpha_{cu}\theta_{cu}\right)\left(L_a + L_e\right)}} \tag{23}$$

Based on the winding temperature constraint, it can be seen from Eq. (23) that the output torque of the motor has a direct relationship with the thermal resistance of each component under a specific motor size and electromagnetic load. Therefore, the thermal management mode affects the torque output ability of the motor.

V. VERIFICATION AND DISCUSSION OF FINITE ELEMENT METHOD

A. VERIFICATION OF THREE-DIMENSIONAL THERMAL NETWORK MODEL CONSIDERING SECONDARY CIRCULATION

In order to verify the effectiveness and high accuracy of the three-dimensional thermal network model considering secondary circulation, Fluent software was used to solve and analyze the cooling schemes of the prototype with companion-type direct cooling. The motor winding models in the companion-type direct cooling schemes is established according to the actual distribution and winding conditions, and equivalent slot insulation is used to replace various insulating materials such as dipping varnish in the slot and interturn insulation. In order to simulate the airflow inside the motor, the interaction between the rotor and the fixed parts is modeled using the rotating coordinate system in the software to simulate the air convection state between the stator and rotor air gaps and between the end of the part and the end cover [33].

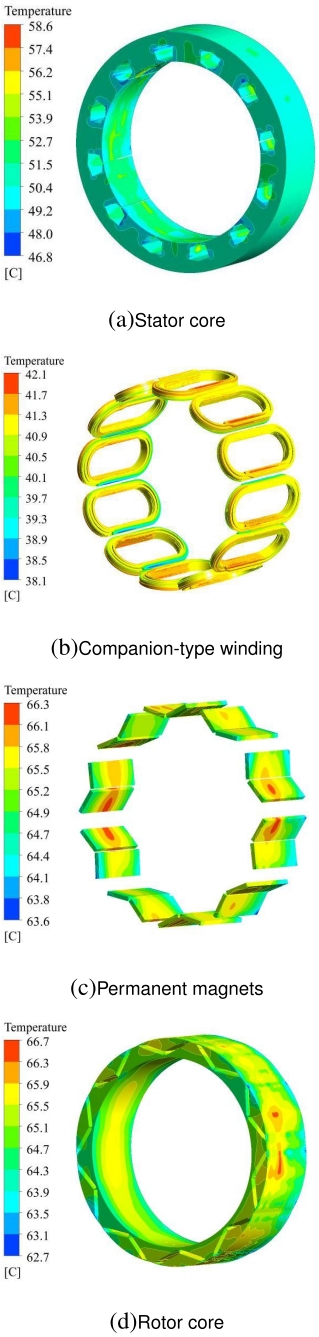

FIGURE 9. Temperature distribution diagram of each component of the companion-type direct cooling motor.

In the companion-type direct cooling scheme, the flow rate and inlet temperature of the cooling medium were set to 0.5m/s and 33°C respectively, while the ambient air temperature was set to 15°C, and the temperature distribution of each component during rated operation of the prototype was simulated. The temperature distribution of each component of the motor based on the companion-type direct cooling scheme is shown in Fig. 9.

A three-dimensional thermal network model (defined as 3D-LTPN1) of the companion-type direct cooling scheme

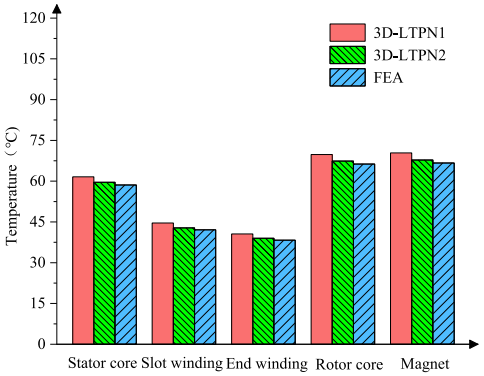

FIGURE 10. Comparison of 3D-LTPN1, 3D-LTPN2 and finite element analysis results.

TABLE 2. Comparison of calculation time and relative error.

Method	Calculation duration(h)	Relative error with FEA(%)
3D-LTPN1	0.12	5.06
3D-LTPN2	0.13	1.63
Finite element	1.17	/

is established in reference [19]. Under the same load and coolant parameters, it is compared with the three-dimensional thermal network model considering secondary circulation (defined as 3D-LTPN2) established in this paper and the finite element temperature field analysis results. The comparison results are shown in Fig.10.

The comparison of 3D-LTPN1, 3D-LTPN2 and finite element method in calculation time, computer resources and calculation accuracy is shown in Table 2.

As can be seen from Fig. 10 and Table 2, compared with the 3D-LTPN1 model, the relative error between the three-dimensional thermal network model (3D-LTPN2) established in this paper and the finite element analysis results is reduced by 3.4%. This is mainly because the three-dimensional thermal network model proposed in this paper not only takes into account the radial-circumferential-axial heat transfer in all directions, but also takes into account the axial lamination of silicon steel sheets and the thermal conductivity of insulating materials in the slot. At the same time, the secondary circulation of the medium in the spiral cooling tube is mainly considered. Therefore, the validity and accuracy of the three-dimensional thermal network model established in this paper are verified, which can accurately reflect the temperature field distribution of the companion-type direct cooling motor in the operation process.

There is little difference between the three-dimensional thermal network model (3D-LTPN2) established in this paper and the 3D-LTPN1 model in terms of computing time and computing resource requirements. When the finite element method is adopted, the calculation time is relatively long, and it takes up a large amount of computing resources. Compared with the finite element method, the three-dimensional thermal network model established in this paper reduces the computing time and computing resources to a great extent. Therefore, the three-dimensional thermal network model considering the secondary circulation established in this paper saves the calculation time and resources under the condition of improving the calculation accuracy, which is of great significance to the follow-up optimization research of the companion-type direct cooling scheme.

B. COMPARISON OF COOLING PERFORMANCE OF TWO THERMAL MANAGEMENT SCHEMES

Under the same load and cooling medium parameters, the temperature distribution of each component of the indirect casing cooling motor during rated operation is simulated and calculated. The temperature distribution cloud diagram of each component of the motor is shown in Fig.11. At the same time, the three-dimensional thermal network analysis method established in this paper is used to analyze and solve the temperature of each component of the motor based on the indirect casing cooling scheme. The calculation results of the finite element and three-dimensional thermal network analysis methods of the two thermal management schemes are compared as shown in Fig.12.

It can be seen from Fig.11 and Fig.12 that the relative error between the three-dimensional thermal network model considering the secondary circulation factor established in this paper (3D-LTPA2) and the finite element analysis results is 1.71%, indicating that the 3D-LTPA2 model still has high prediction accuracy when performing thermal analysis on motors based on indirect casing cooling schemes. At the same time, it can also be seen that that the temperature of the components of the motor based on the companion-type direct cooling is lower than that of the motor based on the indirect casing cooling, which is mainly due to the low thermal resistance path between the winding hot spot and the cooling medium provided by the companion-type direct cooling scheme, thereby improving the heat dissipation capacity of the motor, thereby reducing the thermal potential energy absorbed by each component before the motor reaches thermal equilibrium, and finally reducing the overall temperature rise level of the motor. Fig.12 also shows the rare phenomenon that the end windings are cooler than the in-slot windings in the companion-type direct cooling scheme, which is mainly due to the fact that the end windings are not in contact with the stator core, compared to the medium in the in-slot cooling tubes, the cooling medium at the stator end has a higher heat absorption rate.

The heat generated in the indirect casing cooling motor passes through the stator core yoke and finally passes to the cooling medium in the casing. The thermal convection between the stator core yoke and the casing is limited. The stator core yoke carries a huge heat transfer task. Most of the heat generated in the companion-type direct motor is transferred to the cooling medium in the cooling duct. Only a small part of the heat is transferred to the casing and distributed to the surrounding environment through the stator core yoke. It can be imagined that the stator core yoke carries a smaller heat transfer task. However, there are insulating materials

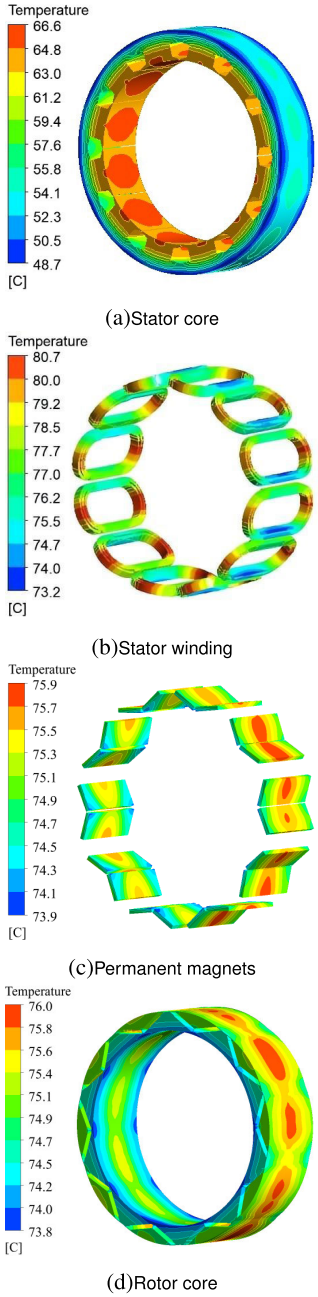

FIGURE 11. Temperature distribution of each component of indirect casing cooling motor.

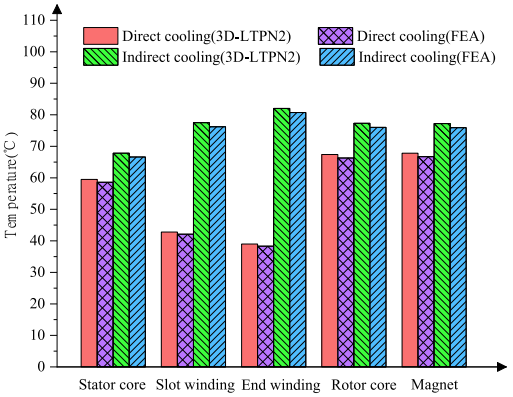

FIGURE 12. Temperature comparison of each part of motor with two cooling schemes.

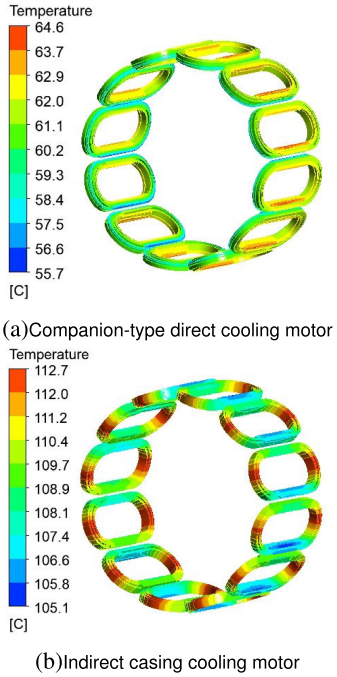

FIGURE 13. The winding temperature distribution of the companion-type direct cooling motor and the indirect casing cooling motor when the load is 4500 N·m.

such as insulating paper and epoxy resin in the stator slot, the thermal conductivity is small, and the heat transferred from the stator core yoke and the stator core teeth to the cooling medium in the slot is limited. Therefore, the stator core temperature rise of the indirect casing cooling scheme is slightly higher than that of the companion-type direct cooling scheme.

Multiple surfaces of the stator slot winding of the companion-type direct cooling motor are in direct contact with the cooling duct, and the stator slot winding is like a bubble in the cooling medium. The heat transfer distance between the stator slot winding of the indirect casing cooling motor and the cooling pipe in the casing is long, and the thermal resistance is large. At the same time, the heat generated by the stator slot winding needs to pass through the slot insulation material with small thermal conductivity. Therefore, the companion-type direct cooling scheme has strong heat dissipation capacity, and the temperature rise of the stator slot winding of the indirect casing cooling scheme is significantly higher than that of the companion-type direct cooling scheme.

VI. EVALUATION OF THE IMPACT-RESISTANCE OVERLOAD CAPABILITY OF THE MOTOR

In industrial production, in order to ensure that the vacuum degree in the vacuum system maintains a certain level, the

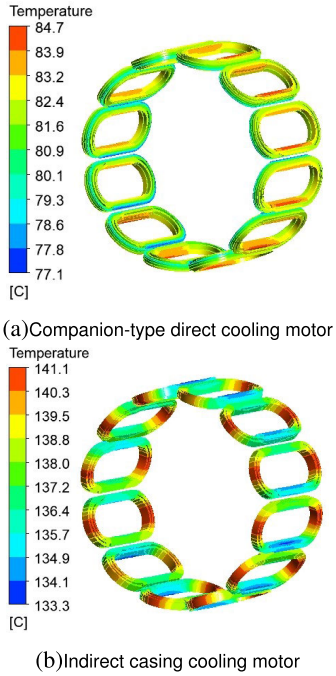

FIGURE 14. The winding temperature distribution of the companion-type direct cooling motor and the indirect casing cooling motor when the load is 5000 N·m.

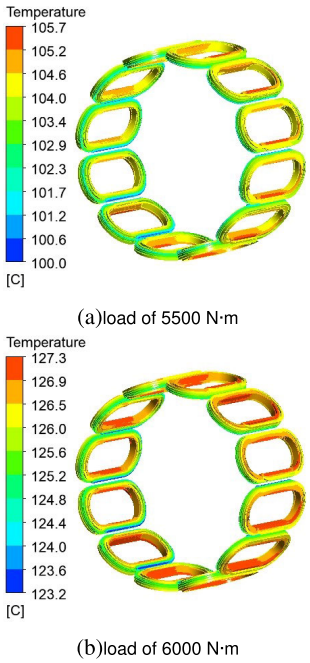

FIGURE 15. The winding temperature distribution of the companion-type direct cooling motor when the load is 5500 N·m and 6000 N·m respectively.

vacuum pump and the motor are often designed into an integrated structure. As the power core of the vacuum dry pump unit, the performance of the drive motor directly affects the overload capacity, vibration noise, ultimate vacuum degree and energy consumption level of the vacuum dry pump. When the motor capacity is certain and runs in the rated state, the temperature rise is usually certain. Therefore, the temperature rise of the motor is closely related to the capacity and working state of the motor. The temperature rise of the motor is very important for the design and operation of the motor. Therefore, it is of great significance to determine the temperature rise limit of the motor and evaluate the load capacity of the motor in combination with the specific conditions and the particularity of the motor working conditions and the special purpose of the motor.

Due to the complex operating conditions of the vacuum pump, the leakage rate in the vacuum system may increase instantaneously due to mechanical reasons or system failures during the stable operation stage of the motor. When the impact load is within the maximum torque range of the motor, this sudden increase in the load may cause the motor to continue to overload, and the motor will produce an overload torque greater than the rated torque. As the current increases, the temperature rise of the motor will also increase, which can easily cause the motor to overheat or even damage the motor, resulting in certain economic losses. Therefore, according to the different requirements of the motor in requirements of the motor, the quantitative calculation of the impact resistance of the motor under different working conditions under the temperature rise limit of the motor can realize the exploration of the load potential of the motor to meet the special working conditions of the vacuum pump motor and prevent the motor from overheating. It has very important theoretical value and practical engineering significance [23].

In order to explore the influence of the heat dissipation conditions of the stator winding on the overload capacity of the motor when the impact load occurs, the three-dimensional thermal network model established in this paper is used to quantitatively calculate the temperature field under the impact load with different load rates, and the finite element analysis is used to verify the applicability of the thermal network model under complex and variable working conditions.

Based on the calculation results of the temperature field of the indirect casing cooling and the companion-type direct cooling motor under the rated state, it can be seen that there is still a safety margin for the winding temperature, and the load capacity of the motor needs to be further explored. Therefore, based on the calculation results of the temperature field under the rated conditions of the motor, the impact load is simulated by setting the overload torque, and the load torque is increased by 500N·m one by one. The calculation result is used as the initial condition of the next simulation calculation, and after comparing with the maximum torque of the motor to determine that the motor has no risk of stalling, the temperature field of the motor under each overload torque is calculated in turn. The temperature rise of the winding hottest point of the motor based on indirect casing cooling and companion-type direct cooling under impact loads with different load rates is obtained. The temperature distribution of the winding under different load torques based on the two thermal management schemes (finite element calculation) is shown in Fig.13-Fig.15.

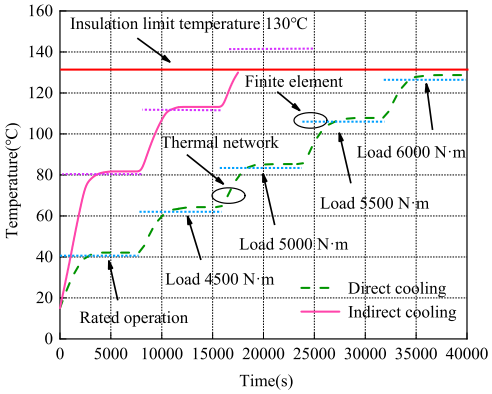

FIGURE 16. Comparison of impact-resistance overload capability under two cooling conditions.

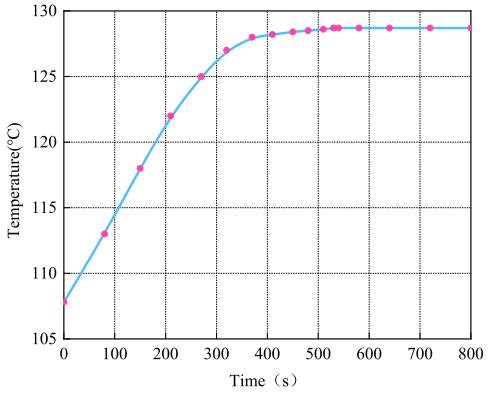

FIGURE 18. Temperature rise curve of winding hottest spot near maximum torque based on companion-type direct cooling scheme.

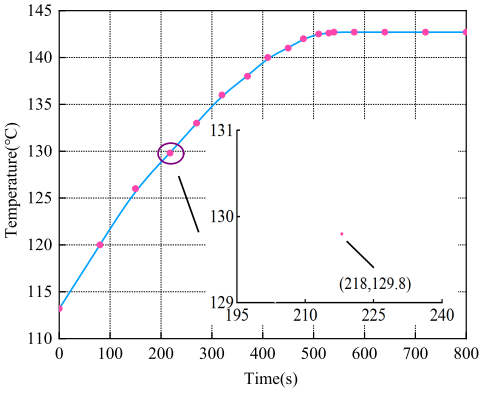

FIGURE 17. Temperature rise curve of winding hottest spot at load 5000N m based on indirect casing cooling scheme.

The analysis and comparison results of the hottest spots of the windings of the two thermal management schemes by the finite element method and the 3D-LTPA2 method are shown in Fig.16. The temperature rise curve of the winding hottest point under the load of 5000N·m of the motor based on the indirect casing cooling scheme is shown in Fig.17. The temperature rise curve of the winding hottest point under the maximum torque of the motor based on the companion-type direct cooling scheme is shown in Fig.18.

It can be seen from Fig.16 that the error between the 3D-LTPA2 and the finite element analysis of the hottest spot analysis of the winding based on the two thermal management schemes under different working conditions is very small, which verifies the applicability and accuracy of the three-dimensional thermal network model considering the secondary circulation factor proposed in this paper under the complex and variable working conditions of the motor. At the same time, it can be seen from Fig.16-Fig.18 that when the motor load increases to the maximum torque of 6000N·m, the steady-state temperature of the hottest spot of the winding based on the companion-type direct cooling scheme has not yet reached the insulation limit temperature of 130°C. However, when the torque increases to 5000N·m, the steady-state temperature of the hottest spot of the winding based on the indirect casing cooling scheme has exceeded the insulation limit temperature after 2.9 minutes, and the motor continues to run there will be security risks, so it shows that the motor based on the companion-type direct cooling scheme has a stronger impact-resistance overload capability. At the same time, it can be seen that the motor based on the companion-type direct cooling is close to the insulation limit temperature under the maximum electrical load. In the future work, the cooling system can be optimized to ensure the safe and stable operation of the motor under the impact load of the maximum torque.

Time required for winding temperature rise to reach steady state under different overload torque based on two cooling schemes are listed in Table 3. It can be seen that under the same electrical load, the time required for the temperature rise of the winding to reach a steady state is shorter in the companion-type direct cooling scheme than in the indirect casing cooling scheme, which further illustrates the high heat dissipation efficiency of the companion-type direct cooling scheme.

Under the same slot filling rate and electrical load, the stator winding cross-sectional area per turn based on the companion-type direct cooling scheme is 1/2 times that based on the indirect casing cooling scheme. The companion-type direct cooling scheme has a smaller winding cross-sectional area, resulting in higher current density. However, it can be seen from Fig.11 that the stator winding temperature based on the companion-type direct cooling scheme is about 1/2 times that of the indirect casing cooling scheme under the rated operating condition of the motor. The strong heat dissipation capacity of the companion-type direct cooling scheme greatly reduces the temperature rise of the winding and other components. Therefore, it can be seen from Eq. (14) that the companion-type direct cooling scheme and the indirect casing cooling scheme have the same resistance value of each phase winding, and the copper loss of the stator winding of the two cooling schemes is the same under the

TABLE 3. Time required for winding temperature rise to reach steady state under different overload torque based on two cooling schemes.

Load torque (N·m)	Winding current (A)	Temperature rise stabilization time (s)		Steady state temperature of winding (°C)	
		Direct	Indirect	Direct	Indirect
4000	288	458	525	42.8	82
4500	330	452	518	65.7	114.6
5000	374	461	510	86.1	143.4
5500	421	462	—	107.4	—
6000	465	450	—	129.4	—

same current of each phase. Therefore, the companion-type direct cooling scheme has little effect on motor loss and other electrical properties.

VII. EXPERIMENT VERIFICATION OF SIMULATED PROTOTYPE

The power loss and related thermal behavior of AC windings strongly depend on various design factors, including the geometry of the stator slot, conductor type, conductor material, conductor layout, and distance from the cooling source. It is therefore not possible to provide generic and universal guidelines regarding discussed power loss and thermal effects as these are strongly driven by a particular application. Therefore, in order to evaluate the thermal envelope for a new motor design, a number of tests on a prototype machine are usually required. As the design process tends to involve a series of iterations, this may require more than one prototype machine to be manufactured and tested. Such an approach can be expensive and time consuming.

In order to provide accurate temperature prediction, the thermal behavior of different parts of the motor can be predicted by manufacturing a simulated machine during the design process. A simulated machine is a representative subassembly of the stator and winding, manufactured using materials and processes commonly used in construction of the final electrical machine prototype. At the same time, the simulated machine subassemblies are less costly and easier to prototype, allowing multiple batches to be produced and compared. At the same time, the ability to predict thermal behaviour in simulation is highly desirable, in order to reduce the overall design cycle by producing an optimised machine with the first prototype iteration. These have proven to be a time- and cost-effective way to calibrate the thermal model of the complete machine component before manufacturing the final design. At the same time, a thermal test on a complete prototype machine is an essential part of the design process. However, for the centralized stator winding design, a test-informed thermal analysis on a single stator tooth can be performed prior to the manufacture of the full machine. This approach allows for a rapid and inexpensive assessment of the thermal performance of the complete machine and early identification of design modifications needed. In references [26], [34], [35], [36], [37], [38], [39], and [40], a simulation machine representing the prototype machine was manufactured, and the method used in the design process was verified by the data of the simulation test. The theoretical results are in good agreement with the experimental results.

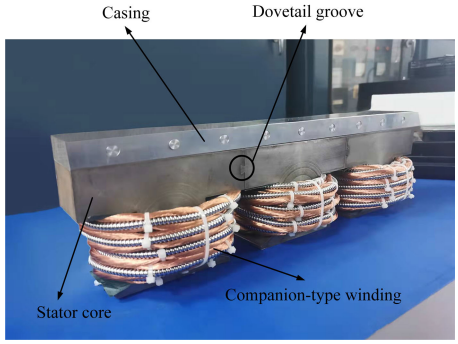

FIGURE 19. Simulation prototype of the companion-type direct cooling scheme.

In order to facilitate the test and verification of the companion-type direct cooling scheme, a simulated prototype structure is designed in this paper, as shown in Fig.19, including the stator core structure, companion-type windings and casing. The designed simulation prototype is in the shape of a cuboid, the stator slots are parallel slots, and the three stator teeth are spliced by dovetail groove, which is convenient for the winding of the companion-type winding. At the same time, the companion-type winding of the prototype adopts the same winding method as the previous one.

In order to compare and verify the companion-type direct cooling and indirect casing cooling, nine circular groove are axially designed in the casing part of the simulated prototype. The windings in the stator slots are wound with four copper conductors in parallel, and the cooling conduits are spirally wound along the circular groove to simulate the indirect casing cooling scheme. The designed structure is shown in Fig.20.

In order to simulate the real operating environment of the motor, the whole simulation motor structure is placed in the foam box, and only the shell surface is exposed to the external environment to simulate the approximate adiabatic environment of the companion-type hybrid coil in the stator slot. At the same time, in order to prevent the copper conductor and the cooling conduit from being separated from each other when the ends are wound in dislocation, the companion-type hybrid coil is fixed with self-locking nylon binding tapes at intervals to ensure that the four parallel copper conductors

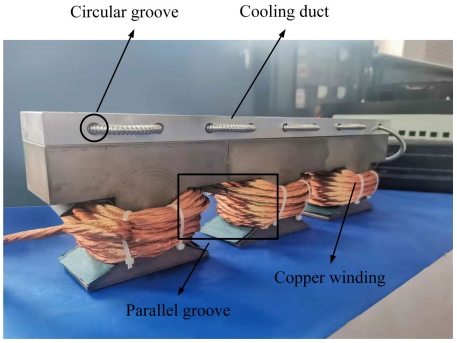

FIGURE 20. Simulation prototype of indirect casing cooling scheme.

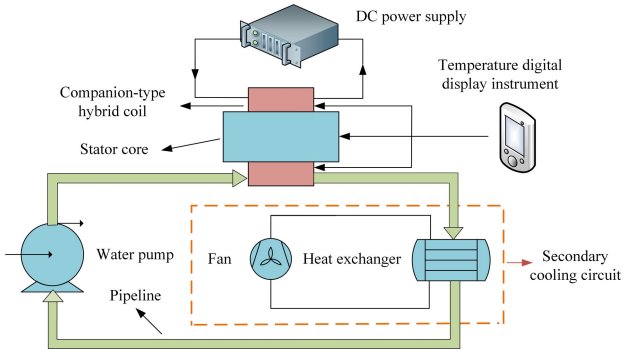

FIGURE 21. Block diagram of the overall test scheme of the simulated prototype.

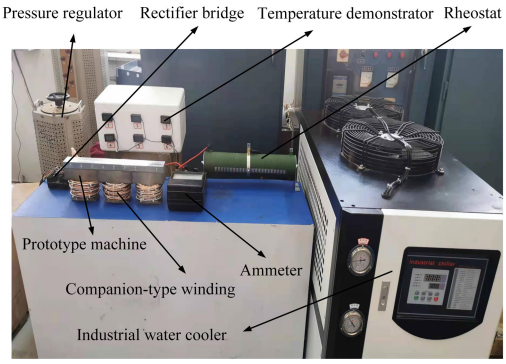

FIGURE 22. Test device for two cooling schemes.

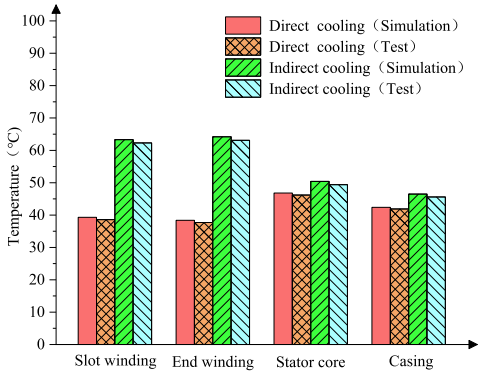

FIGURE 23. Comparison of simulation and test values based on two heat management schemes.

and cooling pipes are distributed according to the design scheme during the whole winding process.

Fig.21 shows the overall test scheme of the simulated prototype, the cooling circuit consists of a primary circuit through cooling conduits, a heat exchanger and a water pump, and a secondary circuit operating as a heat exchanger. In the simulation test, the industrial water cooler is used to cool the water medium, which can not only achieve the same operation effect, but also accurately control the inlet temperature and flow rate of the cooling medium. The copper conductor in the companion-type hybrid coil is supplied with the test current by a three-phase auto-voltage regulator and rectifier bridge.

The experimental test device for the companion-type direct cooling scheme and the indirect casing cooling scheme is shown in Fig.22. Multiple pt100 sensors are embedded in the circumferential and axial positions of the stator slot and end winding, and the most hot spots of the stator winding are directly determined by the temperature display. In order to simulate and compare the heat dissipation capacity of the two cooling schemes during the actual rated operation of the motor, based on the volume relationship between the simulated prototype and the actual prototype, the conductor current supplied by the power supply equipment in the two cooling schemes is 35A during the test. Each temperature display was recorded every 5 minutes until the temperature stabilized. Take the steady-state temperature indication at the hottest spot of the winding as the maximum temperature of the winding, and take the steady-state average of the indications in the slot and end temperature indicators as the average temperature of the slot winding and the end winding.

In order to use the test device to verify the accuracy of the three-dimensional thermal network model considering the secondary circulation for the thermal evaluation of the motor, the three-dimensional thermal network model is used to model the simulation prototype under two thermal management schemes, and the thermal analysis is carried out. The simulation analysis and test of the simulation prototype under the two thermal management schemes are carried out under the same coolant inlet temperature and flow rate at the ambient temperature of 13.8 °C. Fig.23 shows the simulation analysis and test results of the simulation prototype based on the two thermal management schemes.

As can be seen from Fig.23, the simulation analysis values of the simulation prototype based on the two thermal management schemes are very close to the experimental results, which further verifies the accuracy of the three-dimensional thermal network model considering secondary circulation proposed in this paper. At the same time, Fig.23 also shows that the maximum temperature rise of windings in the companion-type direct cooling and indirect casing cooling

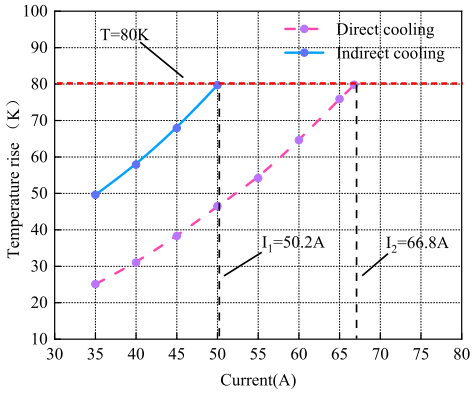

FIGURE 24. Maximum winding temperature of two cooling schemes under different test currents.

schemes is more than 24K, which verifies the heat dissipation advantage of the companion-type direct cooling scheme on the windings. At the same time, it can be seen that the hottest spot in the indirect casing cooling scheme is at the end of the winding, and the hottest spot in the companion-type direct cooling scheme is the winding in the slot. Therefore, the companion-type direct cooling system can not only significantly reduce the temperature of the winding in the slot, but also solve the problem that the end winding is difficult to dissipate heat.

In order to study the heat dissipation potential of the companion-type direct cooling scheme compared with the indirect casing cooling scheme, a current meter is connected in series in the test circuit, and the test current in the conductor is visually displayed by adjusting the three-phase self-coupled voltage regulator, so as to predict the load potential when the companion-type direct cooling scheme is applied to the actual motor. The highest temperature rise of winding in the cooling schemes of the companion-type direct cooling scheme and the indirect casing cooling scheme under different test currents in Fig.24.

It is worth mentioning that the main purpose of the companion-type direct cooling scheme is to reduce the temperature of the winding hottest spot to achieve higher torque density. Based on the insulation grade design of the simulated prototype, the upper limit of the temperature rise of the windings in the simulated prototype is 80K. As can be seen from Fig.24, when the test current is 50.2A, the maximum temperature rise of the windings in the indirect casing cooling scheme is close to the limit of 80K. However, when the companion-type direct cooling scheme is used, the highest steady-state temperature rise of the winding under this current is only 46.5K, and when the test current is 66.8A, the highest temperature of the winding is close to the upper limit of the temperature rise.

Although the simulation test cannot verify the temperature rise process and steady-state temperature of the winding in the simulation analysis of the real prototype, it can effectively verify the efficient heat dissipation capability of the companion-type direct cooling scheme compared with the indirect casing cooling scheme. Because the output torque is proportional to the current, the simulation test also accurately verifies that the companion-type direct cooling scheme can excavate the load potential of the motor to a large extent compared with the indirect casing cooling scheme without exceeding the temperature rise limit of the insulation system.

VIII. CONCLUSION

Based on the limitation of thermal limit on the impact-resistance overload capability of the motor, this paper proposes a thermal management scheme of companion-type direct cooling, establishes a high-precision three-dimensional thermal network model considering secondary circulation to evaluate the impact-resistance overload capability of an example motor, and compares it with the thermal management scheme of indirect casing cooling. The following conclusions were drawn:

1) Through the thermal network analysis, it can be seen that the hottest temperature of the winding in the companion-type direct cooling scheme is 50% of that in the indirect casing cooling under rated operating conditions, showing efficient heat dissipation capacity, which creats a thermal safety condition for improving the overload capacity of the motor under the impact load.

2) Through the simulation comparison between thermal network and finite element under rated working conditions, compared with the three-dimensional thermal network model established in reference [19], the relative error between three-dimensional thermal network established in this paper and finite element analysis results is reduced by 3.4%, and the relative error is 1.63%. At the same time, the simulation time of the three-dimensional thermal network is only 11.1% of that of the finite element, which greatly shortens the calculation cycle without affecting the calculation accuracy of the temperature field, which is beneficial to engineering applications.

3) Through the simulation calculation of the temperature field under the impact load condition, it can be seen that the overload capacity of the companion-type direct cooling scheme is increased by 20% compared with the indirect casing cooling scheme. At the same time, the indirect casing cooling motor can run safely for 2.9 minutes under the condition of 1.25 times the load rate. For the working conditions where the impact load is close to the maximum torque, the companion-type direct cooling motor can still run safely for a longer time, and it has a stronger impact-resistance overload capability.

4) Through the simulation test of two thermal management schemes, the validity of the simulation calculation for the evaluation of load potential is verified. This research provides a new idea for the exploration of the motor's load potential under special working conditions, and also provides a scientific basis for more accurate determination of the reserved window period of the motor overheat protection device under extreme working conditions.

REFERENCES

[1] G.-H. Zhou, M.-Z. Qiao, X.-F. Zhang, J.-H. Xie, Q.-L. Hao, C. Wan, and Y. Zhou, "Development of a low-speed high-efficiency PMSM and its drive system for electric windlass and mooring winch," *IEEE Access*, vol. 10, pp. 70620–70629, 2022.

[2] V. Madonna, P. Giangrande, and M. Galea, "Influence of insulation thermal aging on the temperature assessment in electrical machines," *IEEE Trans. Energy Convers.*, vol. 36, no. 1, pp. 456–467, Mar. 2021.

[3] Z. Hao, J. Shuanbao, W. Dong, W. Gongbao, and H. Pengfei, "Design and analysis of the integrated motor cooling system for shaftless propeller," *IEEE Access*, vol. 7, pp. 174573–174582, 2019.

[4] P. Lindh, I. Petrov, P. Immonen, J. Pyrhonen, M. Niemela, J. Anttila, M. Paakkinen, and E. Scherman, "Performance of a direct-liquid-cooled motor in an electric bus under different load cycles," *IEEE Access*, vol. 7, pp. 86897–86905, 2019.

[5] S. Mizuno, S. Noda, M. Matsushita, T. Koyama, and S. Shiraishi, "Development of a totally enclosed fan-cooled traction motor," *IEEE Trans. Ind. Appl.*, vol. 49, no. 4, pp. 1508–1514, Jul. 2013.

[6] Q. Chen, H. Shao, J. Huang, H. Sun, and J. Xie, "Analysis of temperature field and water cooling of outer rotor in-wheel motor for electric vehicle," *IEEE Access*, vol. 7, pp. 140142–140151, 2019.

[7] S. Nategh, Z. Huang, A. Krings, O. Wallmark, and M. Leksell, "Thermal modeling of directly cooled electric machines using lumped parameter and limited CFD analysis," *IEEE Trans. Energy Convers.*, vol. 28, no. 4, pp. 979–990, Dec. 2013.

[8] J. Huang, "A hybrid electric vehicle motor cooling system—Design, model, and control," *IEEE Trans. Veh. Technol.*, vol. 68, no. 5, pp. 4467–4478, May 2019.

[9] P.-O. Gronwald and T. A. Kern, "Traction motor cooling systems: A literature review and comparative study," *IEEE Trans. Transport. Electrific.*, vol. 7, no. 4, pp. 2892–2913, Dec. 2021.

[10] J. Montonen, J. Nerg, M. Polikarpova, and J. Pyrhonen, "Integration principles and thermal analysis of an oil-cooled and -Lubricated permanent magnet motor planetary gearbox drive system," *IEEE Access*, vol. 7, pp. 69108–69118, 2019.

[11] A. Santisteban, A. Piquero, F. Ortiz, F. Delgado, and A. Ortiz, "Thermal modelling of a power transformer disc type winding immersed in mineral and ester-based oils using network models and CFD," *IEEE Access*, vol. 7, pp. 174651–174661, 2019.

[12] L. Yan, Z. Dong, and S. Zhang, "Thermal analysis of a novel linear oscillating machine based on direct oil-cooling windings," *IEEE Trans. Energy Convers.*, vol. 37, no. 2, pp. 1042–1051, Jun. 2022.

[13] L. Wang, Y. Li, B. Kou, F. Marignetti, and A. Boglietti, "Influence of ventilation modes on the 3D global heat transfer of PMSM based on polyhedral mesh," *IEEE Trans. Energy Convers.*, vol. 37, no. 2, pp. 1455–1466, Jun. 2022.

[14] P. M. Lindh, "Direct liquid cooling in low-power electrical machines: Proof-of-concept," *IEEE Trans. Energy Convers.*, vol. 31, no. 4, pp. 1257–1266, Dec. 2016.

[15] P. Lindh, I. Petrov, A. Jaatinen-Värri, A. Grönman, M. Martinez-Iturralde, M. Satrústegui, and J. Pyrhönen, "Direct liquid cooling method verified with an axial-flux permanent-magnet traction machine prototype," *IEEE Trans. Ind. Electron.*, vol. 64, no. 8, pp. 6086–6095, Mar. 2017.

[16] X. Jiang, Y. Zhang, S. Jin, F. Zhang, and C. Gerada, "A novel thermal network model used for temperature calculation and analysis on brushless doubly-fed generator with winding encapsulating structure," *IEEE Trans. Ind. Appl.*, vol. 55, no. 2, pp. 1473–1483, Mar. 2019.

[17] W. Yu, W. Hua, J. Qi, H. Zhang, G. Zhang, H. Xiao, S. Xu, and G. Ma, "Coupled magnetic field-thermal network analysis of modular-spoke-type permanent-magnet machine for electric motorcycle," *IEEE Trans. Energy Convers.*, vol. 36, no. 1, pp. 120–130, Mar. 2021.

[18] C. Liu, X. Wang, S. Wang, Y. Wang, G. Lei, and J. Zhu, "Magnetothermal coupling analysis of permanent magnet claw pole machine using combined 3D magnetic and thermal network method," *IEEE Trans. Appl. Supercond.*, vol. 32, no. 6, pp. 1–5, Sep. 2022.

[19] Y. Huang, J. Zhu, and Y. Guo, "Thermal analysis of high-speed SMC motor based on thermal network and 3-D FEA with rotational core loss included," *IEEE Trans. Magn.*, vol. 45, no. 10, pp. 4680–4683, Oct. 2009.

[20] L. Mo, T. Zhang, and Q. Lu, "Thermal analysis of a flux-switching permanent-magnet double-rotor machine with a 3-D thermal network model," *IEEE Trans. Appl. Supercond.*, vol. 29, no. 2, pp. 1–5, Mar. 2019.

[21] A. Boglietti, M. Cossale, S. Vaschetto, and T. Dutra, "Winding thermal model for short-time transient: Experimental validation in operative conditions," *IEEE Trans. Ind. Appl.*, vol. 54, no. 2, pp. 1312–1319, Mar. 2018.

[22] Z. Gao, R. S. Colby, T. G. Habetler, and R. G. Harley, "A model reduction perspective on thermal models for induction machine overload relays," *IEEE Trans. Ind. Electron.*, vol. 55, no. 10, pp. 3525–3534, Oct. 2008.

[23] A. Boglietti, M. Cossale, S. Vaschetto, and T. Dutra, "Experimental validation in operative conditions of winding thermal model for short-time transient," in *Proc. IEEE Energy Convers. Congr. Expo. (ECCE)*, Sep. 2016, pp. 1–6.

[24] X. Fan, R. Qu, B. Zhang, J. Li, and D. Li, "Split ratio optimization of high-speed permanent magnet synchronous machines based on thermal resistance network," in *Proc. 22nd Int. Conf. Electr. Mach. (ICEM)*, 2016, pp. 2059–2065.

[25] Z. Zhu, W. Zhang, Y. Li, and J. Guo, "Thermal analysis of axial permanent magnet flywheel machine based on equivalent thermal network method," *IEEE Access*, vol. 9, pp. 33181–33188, 2021.

[26] V. Madonna, A. Walker, P. Giangrande, G. Serra, C. Gerada, and M. Galea, "Improved thermal management and analysis for stator end-windings of electrical machines," *IEEE Trans. Ind. Electron.*, vol. 66, no. 7, pp. 5057–5069, Jul. 2019.

[27] H. Li and Y. Shen, "Thermal analysis of the permanent-magnet spherical motor," *IEEE Trans. Energy Convers.*, vol. 30, no. 3, pp. 991–998, Sep. 2015.

[28] X. Zhang, C. Zhang, L. Li, J. Cao, and K. Wang, "Split ratio optimization for permanent magnet synchronous machines considering winding temperature limitation," *Trans. China Electrotechnical Soc.*, vol. 34, no. 9, pp. 1886–1899, May 2019.

[29] H. Li, K. W. Klontz, V. E. Ferrell, and D. Barber, "Thermal models and electrical machine performance improvement using encapsulation material," *IEEE Trans. Ind. Appl.*, vol. 53, no. 2, pp. 1063–1069, Mar. 2017.

[30] H. Vansompel and P. Sergeant, "Extended end-winding cooling insert for high power density electric machines with concentrated windings," *IEEE Trans. Energy Convers.*, vol. 35, no. 2, pp. 948–955, Jun. 2020.

[31] W. Tong, R. Sun, S. Li, and R. Tang, "Loss and thermal analysis for high-speed amorphous metal PMSMs using 3-D electromagnetic-thermal bi-directional coupling," *IEEE Trans. Energy Convers.*, vol. 36, no. 4, pp. 2839–2849, Dec. 2021.

[32] S.-O. Kwon, S.-I. Kim, P. Zhang, and J.-P. Hong, "Performance comparison of IPMSM with distributed and concentrated windings," in *Proc. Conf. Rec. IEEE Ind. Appl. Conf. 41st IAS Annu. Meeting*, Oct. 2006, pp. 1984–1988.

[33] S. A. Abdelrahman and B. Bilgin, "Computationally efficient surrogate-based magneto-fluid-thermal numerical coupling approach for a water-cooled IPM traction motor," *IEEE Access*, vol. 10, pp. 83692–83704, 2022.

[34] R. Wrobel, P. H. Mellor, and D. Holliday, "Thermal modeling of a segmented stator winding design," *IEEE Trans. Ind. Appl.*, vol. 47, no. 5, pp. 2023–2030, Sep./Oct. 2011.

[35] R. Wrobel, D. Staton, R. Lock, J. Booker, and D. Drury, "Winding design for minimum power loss and low-cost manufacture in application to fixed-speed PM generator," *IEEE Trans. Ind. Appl.*, vol. 51, no. 5, pp. 3773–3782, Sep./Oct. 2015.

[36] N. Simpson, R. Wrobel, and P. H. Mellor, "Estimation of equivalent thermal parameters of impregnated electrical windings," *IEEE Trans. Ind. Appl.*, vol. 49, no. 6, pp. 2505–2515, Nov. 2013.

[37] J. Godbehere, R. Wrobel, D. Drury, and P. H. Mellor, "Experimentally calibrated thermal stator modeling of AC machines for short-duty transient operation," *IEEE Trans. Ind. Appl.*, vol. 53, no. 4, pp. 3457–3466, Jul./Aug. 2017.

[38] R. Wrobel, A. Mlot, and P. H. Mellor, "Investigation of end-winding proximity losses in electromagnetic devices," in *Proc. 21st Int. Conf. Electr. Mach. (ICEM)*, Sep. 2010, pp. 1–6.

[39] R. Wrobel, P. H. Mellor, D. Salt, and N. Simpson, "Comparative study of copper and aluminium conductors—Future cost effective PM machines," in *Proc. 7th IET Int. Conf. Power Electron., Mach. Drives (PEMD)*, 2014, pp. 1–6.

[40] R. Wrobel, S. J. Williamson, J. D. Booker, and P. H. Mellor, "Characterising the performance of selected electrical machine insulation systems," in *Proc. IEEE Energy Convers. Congr. Expo. (ECCE)*, Sep. 2015, pp. 4857–4864.

QIANG HOU was born in Fenyang, Shanxi, China, in 1993. He received the M.S. degree from the College of Mechanical Engineering, Jiamusi University, Jiamusi, China, in 2020. He is currently pursuing the Ph.D. degree with the College of Electrical Engineering, Shenyang University of Technology, Shenyang, China. His research interests include electromagnetic design, thermal design, and the energetic behaviors of electric machines.

YUEJUN AN was born in Changchun, Jilin, China, in 1962. He received the Ph.D. degree in electrical machine and electrical apparatus from the Shenyang University of Technology, in 2005. He has been a Professor with the College of Electrical Engineering, Shenyang University of Technology, since 2009. His research interests include the design of special motor, the numerical calculation of integrated physical field in motor, the cooling systems of electric motors, and thermal modeling.

MING LI was born in Jinzhou, Liaoning, China, in 1987. He received the M.S. degree from the School of Electrical Engineering, Shenyang University of Technology, Shenyang, China, in 2013, where he is currently pursuing the Ph.D. degree. Since 2013, he has been with Bohai University, as a Lecturer. His research interests include electromagnetic design, thermal design, and the energetic behaviors of electric machines.

HUI AN was born in Shenyang, Liaoning, China, in 1989. He received the B.S. degree from the College of Electrical Engineering, Shenyang University of Technology, Shenyang, in 2012, and the M.S. degree from the College of Information Science and Engineering, Shenyang University of Technology, in 2017. His research interests include motor design and automation control.

NING SUN was born in Jinzhou, Liaoning, China, in 1980. He received the M.S. degree from the College of Electrical Engineering, Shenyang University of Technology, in 2009. Since 2003, he has been with the Shenyang University of Technology, as an Engineer. His research interests include low-speed high-torque permanent magnet electric machine design, permanent magnet wind generator design, and brushless dc motor design.

CHANGLIN LIU was born in Jiamusi, Heilongjiang, China, in 1997. He received the B.S. degree from the Department of Electrical Engineering, Harbin University of Science and Technology, Harbin, China, in 2019. He is currently pursuing the M.S. degree with the College of Electrical Engineering, Shenyang University of Technology, Shenyang, China. His research interests include the design, analysis, and control of electrical machines and industrial machinery.

YANJUN LU was born in Penglai, Shandong, China, in 1990. She received the B.S. and M.S. degrees from the College of Mechanical Engineering and Automation, Northeastern University, Shenyang, China, in 2013 and 2015, respectively. Her research interests include the design and analysis of electrical machines and industrial machinery.